processes

MDPI

Article

Hybrid Cooling-Based Thermal Management of Containerised Vanadium Flow Battery Systems in Photovoltaic Applications

Bing Shu [1], Maria Skyllas-Kazacos [1,*], Jie Bao [1] and Ke Meng [2]

1 School of Chemical Engineering, University of New South Wales, Sydney, NSW 2052, Australia; j.bao@unsw.edu.au (J.B.)
2 School of Electrical Engineering & Telecommunications, University of New South Wales, Sydney, NSW 2052, Australia; ke.meng@unsw.edu.au
* Correspondence: m.kazacos@unsw.edu.au

Abstract: The integration of industrial batteries with photovoltaic applications is a common practice to charge the batteries using solar energy. Long-duration flow batteries are useful in dealing with the intermittency of renewable energy sources and offer a great opportunity for total fossil fuel replacement. In this study, the effects of different battery operation time and load profiles on the temperature dynamics of a containerised vanadium flow battery system are modelled and simulated for a range of locations and seasons to identify active cooling or heating requirements that might be needed to maintain safe operating temperatures. This paper explores and analyses the stack, tank, and container temperature dynamics of 6 h and 8 h containerised vanadium flow batteries (VFBs) during periods of higher charge and discharge current using computer simulations that apply insulation with passive or active hybrid cooling thermal management where needed to keep the battery temperature within a safe operating range under a range of climate conditions. According to the simulation results, when adopting the hybrid cooling strategy as described in the case study, for a 30 kW–240 kWh VFB system with ambient temperatures fluctuating between 25 °C and 45 °C, the monthly electricity consumption of the air conditioning system, calculated using average power, can be maintained at a relatively low level of approximately 330 kWh. By employing an air conditioning system with an airflow rate of 0.2 m^3/s and a suitable thermal management strategy, it is sufficient to keep an 8 h system operating within a safe temperature range when the ambient temperature is between 15 °C and 35 °C. This study presents the first application of our previously developed containerised VFB thermodynamic model to explore the necessity of active cooling or heating in PV (photovoltaic) applications across different geographical locations and seasons. This analysis provides valuable insights for battery designers and manufacturers to understand the performance of containerised battery systems under various climate conditions. Furthermore, this paper is the first to apply this model for simulating 6 and 8 h batteries and to adopt a hybrid thermal management strategy. The simulation data offer guidance on whether active cooling or heating is required for industrialised vanadium batteries with capacities exceeding 6 h.

Keywords: photovoltaic applications; temperature dynamics; thermal management

Citation: Shu, B.; Skyllas-Kazacos, M.; Bao, J.; Meng, K. Hybrid Cooling-Based Thermal Management of Containerised Vanadium Flow Battery Systems in Photovoltaic Applications. *Processes* **2023**, *11*, 1431. https://doi.org/10.3390/pr11051431

Academic Editor: George J. Tsekouras

Received: 7 April 2023
Revised: 2 May 2023
Accepted: 5 May 2023
Published: 8 May 2023

1. Introduction

The vanadium flow battery, invented by UNSW Sydney researchers in the 1980s, has been widely used in a range of power systems. Its applications mainly include peak shaving, valley filling, load levelling, and frequency regulation, as well as renewable energy storage and grid integration. These applications help improve the stability, safety, and reliability of power systems. In ultra-large-scale power grid applications, owing to the fact that the energy of all-vanadium flow batteries (VFBs) is stored in the electrolyte, increasing their energy storage capacity only requires increasing the tank volume to

accommodate more electrolyte. Compared to lithium battery systems, vanadium batteries have a smaller footprint when expanding energy storage capacity and are less prone to catching fire. In addition, in the context of the ongoing global decarbonisation efforts, renewable energy sources have been extensively developed and utilised. However, the majority of renewable energy sources exhibit intermittent characteristics, and spatiotemporal discrepancies persist between the availability of energy supply and the consumption of end users [1]. Thus, vanadium batteries have become increasingly popular in this field for energy storage applications.

To date, a number of thermal models have been developed to study the thermodynamics and thermal behaviour of vanadium battery systems. Tang et al. were the pioneers in proposing a thermodynamic model for vanadium redox flow batteries. Early models did not account for self-discharge [2], and the energy balance of the pipes was also not considered. In subsequent models by Tang et al., thermodynamic models for self-discharge during standby and energy balance equations for pipes were proposed [3]. Later, Yan et al. built upon these models to develop a thermodynamic model for individual cells [4]. After that, Andrea et al. investigated the thermodynamics in industrial-scale vanadium batteries under high current conditions [5]. Nevertheless, the analysis was limited to a single load profile or non-containerised systems. On the other hand, many VFB manufacturers are moving towards containerised systems that can be mass produced and easily configured for different power/energy capacity requirements. A thermal model was recently proposed in [6] for a containerised 4 h VFB system operating in a residential power arbitrage application, which incorporated passive cooling. However, the above work assumed a short discharging time during peak tariff times and fixed overnight charging when electricity prices are low. Active cooling solutions for hot climates were not explored, either. Andrea et al. initially introduced a thermal management method for VFB systems during standby, demonstrating its effectiveness in a kilowatt-class VFB system [7]. Nevertheless, the proposed methods do not offer practical cooling solutions during charging and discharging, and they remain inapplicable to containerised VFB systems. A forced cooling strategy was suggested in [8], which was then contrasted with a nonlinear computational fluid dynamics (CFD) model. Nevertheless, the energy consumption of refrigeration devices was neglected, and hybrid cooling was not studied, nor did the strategy apply to containerised VFB systems as well. Subsequently, a thermal management and control model was proposed by Ankur et al. to enhance system efficiency [9]. However, the system was assumed to be directly exposed to the ambient temperature, leaving the thermal management of containerised VFB systems unexplored.

With the increasing demand for longer duration battery storage systems for renewable energy applications, it is therefore imperative to investigate the temperature dynamics of both the stack and electrolyte tank for a containerised VFB system with storage capacities of over 6 h. Moreover, enhanced temperatures improve electrolyte flow by reducing viscosity, facilitating better contact with electrodes, and thereby augmenting battery performance [10]. However, excessive heat may induce evaporation and compromise the integrity of components. Additionally, elevated temperatures expedite redox reactions, fostering more efficient charge transfer and reducing polarisation losses [11,12]. This results in heightened battery efficiency, albeit at the cost of accelerated degradation and increased safety risks. Moreover, higher temperatures bolster electrolyte conductivity, mitigating ohmic losses and benefiting overall performance [13]. Such benefits must be balanced against potential drawbacks, including electrolyte evaporation, diminished chemical stability, membrane degradation, and thermal stress. Furthermore, ion exchange membrane performance is subject to temperature-related variations in stability, permeability, and selectivity [14]. Therefore, feasible active cooling or heating approaches should be explored for maintaining stack and tank temperatures within a safe operation range to prevent precipitation of V^{5+} and the degradation of the proton exchange membrane (PEM) at elevated temperatures or precipitation of V^{2+}, V^{3+} or VO^{2+} at low temperatures [15].

Moreover, it is important to ensure that the load profiles used in the simulation are representative of the common residential applications with PV systems.

The objective of this paper is to broaden the scope of the thermal studies to include 6 and 8 h containerised vanadium flow battery (VFB) systems integrated with photovoltaic (PV) connected residential loads. In the scenario where the temperature of the stacks and tanks surpasses the acceptable operational range under high ambient temperature conditions when passive cooling proves inadequate, the implementation of an effective air conditioning system will be explored. Considering economic feasibility and the pursuit of maximum benefits, a hybrid cooling method that incorporates both passive and active cooling is employed in this study. The operating time, airflow rate, and power consumption of the air conditioning system will be explored to provide a hybrid cooling solution that can ensure the battery temperature remains within a safe operating range. This will provide insights into the thermal management of containerised VFB systems in different climates and seasons of the year when both ambient temperatures and solar irradiation times vary significantly. This paper will allow battery designers and manufacturers to have an indication of how industrialised vanadium flow batteries perform and whether these batteries need active and/or passive cooling under different climate conditions.

In Section 2, an overview of the relevant reactions, simulation models, assumptions, and hybrid cooling strategies for the containerised vanadium redox flow batteries (VRFBs) is provided. Section 3 elaborates on the specific parameters required for the simulations, the various loading profiles used and their rationale, as well as the control logic. For different loading profiles, a pioneering containerised VRFB thermodynamic model, which was initially proposed by the authors, is applied for the first time to simulate PV-related applications in different regions and seasons. The simulation results are presented and analysed in the case studies. In the discussion section, the specific content of the simulations is outlined. Section 4 summarises the entire paper and presents the conclusions drawn from the application of the methods described. This provides valuable simulation support for determining the need for active and passive cooling in the industrialised VRFB PV-related applications and analyses the electricity consumption of the air conditioning systems in the described applications.

2. Thermal Model and Chemical Reactions for the Containerised VFB System

Vanadium flow batteries utilise the four valence states of vanadium ions to achieve rechargeability through redox reactions involving the gain and loss of electrons. The specific reactions are shown as follows.

At the positive side:

$$VO_2^+ + 2H^+ + e^- \underset{\text{charge}}{\overset{discharge}{\rightleftharpoons}} VO^{2+} + H_2O, E^0 = +1\ V \quad (1)$$

At the negative side:

$$V^{3+} + e^- \underset{\text{discharge}}{\overset{charge}{\rightleftharpoons}} V^{2+} + 2H^+ + e^-, E^0 = -0.26\ V \quad (2)$$

Capacity degradation and self-discharge in vanadium redox flow batteries occur during both standby periods and charging/discharging processes, mainly as a result of the permeation of vanadium ions across the membrane. Although permeation occurs all the time, the absence of active pumping during the standby period exacerbates the self-discharge issue as the heat generated by the process is not efficiently extracted. During standby periods when the pumps are turned off, heat is generated inside the stacks because of the self-discharge reactions, leading to increased stack temperatures that in turn increase the rate of vanadium ion diffusion across the membrane [3]. The main self-discharge reactions are presented below.

At the negative side (because of VO_2^+ and VO^{2+} diffusion):

$$VO_2^+ + 2V^{2+} \rightarrow 3V^{3+} \quad (3)$$

$$VO^{2+} + V^{2+} \rightarrow 2V^{3+} \quad (4)$$

$$VO_2^+ + V^{3+} \rightarrow 2VO^{2+} \quad (5)$$

At the positive side (because of V^{2+} and V^{3+} diffusion):

$$V^{2+} + 2VO_2^+ \rightarrow 3VO^{2+} \quad (6)$$

$$V^{3+} + VO_2^+ \rightarrow 2VO^{2+} \quad (7)$$

$$V^{2+} + VO^{2+} \rightarrow 2V^{3+} \quad (8)$$

2.1. Simulation Assumptions

In this study, simulations were based on several assumptions, as shown below:

1. The electrolyte is completely filled in the tanks.
2. The temperature and concentration distribution within the system is uniform.
3. The containerised system is shaded so radiant heating can be ignored.
4. No gassing side reactions occur.
5. The stack design minimises shunt currents, so that the effect of shunt currents can be ignored.
6. The resistance of the stacks remains consistent.
7. The tanks as well as stacks are modelled as Continuous Stirred Tank Reactors (CSTRs).
8. Reactions (4) and (7) are assumed negligible.
9. Of the heat generated by the pumps, 50% is dissipated into the air within the container, and the rest is dissipated into the electrolyte.
10. The insulation material is placed between two metal sheets that make up the walls of the container.
11. The two side surfaces of the two tanks are in contact with each other, while the other three side walls are in direct contact with the walls of the container.

2.2. Mass Balance and Energy Balance of the Containerised VFB System

The mass balance and energy balance equations for the containerised VFB system employed in this study were consistent with the model presented in [2–4]. Additionally, the Arrhenius equation was utilised to incorporate the temperature dependency of the membrane diffusion coefficients.

2.3. Hybrid Cooling and Auxiliary Heating for Containerised VFB System

The safe operating temperature range for the electrolyte in the stacks and tanks is between 10 °C and 40 °C to ensure optimal performance and avoid electrolyte precipitation. As the operating time and current of the battery system increases, ohmic heating becomes a significant concern, resulting in a continuous elevation of temperature in the stacks and tanks. Hence, solely employing fan-based passive cooling may prove inadequate in lowering the temperature of the stacks and tanks in specific ambient temperature scenarios. Such circumstances demand the implementation of additional cooling techniques for effective thermal management. In this paper, a hybrid cooling strategy was implemented where an air conditioning system was switched on when passive fan cooling was insufficient in controlling the battery temperature. Compared to other types of cooling/heating apparatus (e.g., water cooling systems), air conditioning systems offer flexibility, simplicity, lower maintenance, and no risk of water damage. Air conditioners can

maintain a wide range of target temperature and humidity levels and can run in both active and passive cooling (fan only) modes.

2.3.1. Hybrid Cooling Strategy

For varying ambient conditions, fan-based passive cooling has greater efficacy during periods of relatively lower ambient temperatures within each day. Nonetheless, as ambient temperature increases, the cooling efficiency of fan-based passive cooling systems will be constrained by the ambient temperature. Therefore, to maintain stack and tank temperatures within the normal operating range, the implementation of active cooling during periods of high ambient temperatures is imperative. The equations describing the rates of heat transfer for passive and active cooling are presented below.

For fan-based passive cooling:

$$Q_{fans} = -N_{fans}\dot{m}C_{p,air}(T_{air,in} - T_{air}) \quad (9)$$

where N_{fans} is number of fans, $\dot{m}$ ($air\ density \times airflow\ of\ the\ fan$) is mass flow rate of the air (kg/s), $C_{p,air}$ is the specific heat of the air (J/(kg·K)), T_{air} is the ambient temperature (K), $T_{air_{in}}$ is air temperature inside the container (K).

The expression of the fan-based cooling formula is based on the principle of conservation of heat and the thermal properties of air. In a closed system, the total amount of heat is constant. If one part of the system absorbs heat, the other part must lose the same amount of heat. The fan airflow rate refers to the volume of air that the fan can circulate per unit of time. It directly affects the heat exchange capacity of the fan-based cooling system. The higher the airflow rate, the better the cooling effect. Air density (ρ) and specific heat capacity ($C_{p,air}$ in J/(kg·K) are thermal property parameters of air. These parameters describe the heat conduction characteristics of air during the absorption and release of heat. The temperature difference (K) represents the difference between the air temperature inside the container and ambient temperature. This parameter reflects the heat absorption capacity of the air in the fan-based cooling system. The larger the temperature difference (i.e., the cooler the outside air), the stronger the heat transfer capacity. Additionally, it should be noted that fan-based passive cooling relies on ambient temperature. Although properly increasing the airflow rate can enhance the cooling effect, this effect is still limited by the ambient temperature [6].

For air conditioning-based active cooling:

$$Q_{active-cooling} = -\dot{V} \times \rho \times C_{p,air} \times (T_{air_{in}} - T_{cold-air}) \quad (10)$$

where $\dot{V}$ is the airflow rate (m^3/s), ρ is air density (kg/m³), $T_{air_{in}}$ is the air temperature inside the container (K), $C_{p,air}$ is the specific heat of air (J/(kg·K)), and $T_{cold-air}$ is the cold air temperature coming from air conditioning system (K). Commercial air conditioning systems are characterised by various parameters, such as airflow rate and power consumption.

Similarly, Equation (10) is based on the first law of thermodynamics, which is the law of conservation of energy. This equation describes the heat transfer capacity of an air conditioning system. $T_{air-in} - T_{cold-air}$ is the temperature difference between the air entering and leaving the air conditioning system. By incorporating the temperature difference between the inlet and outlet air into the formula, the heat transfer capacity (Q) of the air conditioning system can be determined.

2.3.2. Heating Generated by Pumps and Power Electronic Devices

Inverters are used as DC–AC converters in photovoltaic-connected battery systems for power conversion. In containerised systems, pumps play an important role in transferring the electrolyte from the tanks to the stacks. In these simulations, it was assumed that half of the heat generated by the pumps contributed to the air inside the container,

while the other half contributed to the electrolyte. If inverters are not isolated from the inner environment, the heat generated by them will directly contribute to the air temperature inside the container. Studies have shown that allowing the heat generated by inverters to directly contribute to the inner environment can cause a continuous increase in the internal temperature [6]. They therefore need to be isolated from the inner environment for normal or hot climate scenarios. The equations for calculating heat generated by pumps and inverters are presented in [6].

3. Simulation and Results

This study analysed the simulation results for containerised VFB systems with capacities of 30 kW–180 kWh and 30 kW–240 kWh. The aim of the analysis was to evaluate the temperature response of important components within these systems under various ambient temperature conditions and provide hybrid cooling suggestions for stationary energy storage applications. The Fundtech FAP-450 membrane [16–18] was utilised in all simulations. Hybrid cooling was implemented as needed in various ambient temperature scenarios.

3.1. System Specifications

As partly presented in [4], the design parameters and system components are shown in Table 1. Table 2 displays the diffusion coefficients of vanadium ions for this membrane [19].

Table 1. Specifications of the system.

Parameter	Symbol	Value
Volume of each tank (6-h battery)	V_{tank1}	4.997 m^3
Volume of each tank (8-h battery)	V_{tank2}	6.663 m^3
Height of each tank (6-h battery)	H_{tk1}	0.9748 m
Height of each tank (8-h battery)	H_{tk2}	1.2998 m
Volume of each stack	V_{stack}	10.3 L
Number of stacks		20
Volume of each pipe (tank to stack)	V_{pipe1}	2.4261 dm^3
Volume of each pipe (tank to stack)	V_{pipe2}	3.7561 dm^3
Flow rate factor	Q_f	2
Total vanadium concentration	c	1.6 mol/L
Specific heat of electrolyte	C_ρ	3.2 $Jg^{-1}K^{-1}$
Density of electrolyte	ρ	1354 kgm^{-3}
Thickness of tank walls	θ	0.01 m
Tank wall material heat transfer coefficient (polyethylene)	k_{tank}	0.34 $Wm^{-1}K^{-1}$
Stack flow frame thermal conductivity (polytetrafluoroethylene)	k_{stack}	0.3 $Wm^{-1}K^{-1}$
Membrane area	S	1000 cm^2
Membrane thickness	d	1.27×10^{-4} m
Activation energy for diffusion	E_a	17,341 $Jmol^{-1}$
Reaction (6) enthalpy change	$\Delta H_{(1)}$	-220 kJ mol^{-1}
Reaction (7) enthalpy change	$\Delta H_{(2)}$	-64 kJ mol^{-1}

Reaction (4) enthalpy change	$\Delta H_{(4)}$	-91.2 kJ mol^{-1}
Reaction (3) enthalpy change	$\Delta H_{(5)}$	-246.8 kJ mol^{-1}
Overall heat transfer coefficient of from side walls to air of each tank (no insulation)	$U_{t_{sd1}}$	1.896 Wm^{-2}K^{-1}
Overall heat transfer coefficient of from bottom walls to ground (no insulation)	$U_{t_{bt}}$	2.756 Wm^{-2}K^{-1}
Overall heat transfer coefficient of from side walls to air of each tank (with 0.02 m insulation)	$U_{t_{sd2}}$	0.753 Wm^{-2}K^{-1}
Overall heat transfer coefficient of from bottom walls to ground (with 0.02 m insulation)	$U_{t_{bt2}}$	0.86 Wm^{-2}K^{-1}
Overall heat transfer coefficient of from top wall to inner air of each tank	$U_{t_{tp}}$	4.45 Wm^{-2}K^{-1}
Overall heat transfer coefficient of side walls of each stack	U_{s1}	1.88 Wm^{-2}K^{-1}
Overall heat transfer coefficient of from bottom walls to ground (with 0.02 m insulation)	U_{s2}	3.13 Wm^{-2}K^{-1}
Gas constant	R	8.314 Jmol^{-1}K^{-1}
Overall heat transfer coefficient of the container (steel side walls, no insulation)	U_{con1}	2.04 Wm^{-2}K^{-1}
Overall heat transfer coefficient of the outer container walls to air (steel top wall, no insulation)	U_{con2}	3.06 Wm^{-2}K^{-1}
Overall heat transfer coefficient of the container (side walls with 0.02m insulation)	U_{con3}	0.775 Wm^{-2}K^{-1}
Overall heat transfer coefficient of the container	U_{con4}	0.887 Wm^{-2}K^{-1}
Pipe length (each)	L	4.5 m
Pipe diameter (tanks to stacks)	θ_{pipe1}	0.032 m
Pipe diameter (stacks to tanks)	θ_{pipe2}	0.040 m
Pipe thickness (tanks to stacks)	$D1$	0.0058 m
Pipe thickness (stacks to tanks)	$D2$	0.0074 m
Overall heat transfer capability of pipes (tanks to stacks)	$U_{p1}A_{p1}$	2.62 WK^{-1}
Overall heat transfer capability of the pipes (stacks to tanks)	$U_{p2}A_{p2}$	3.02 WK^{-1}
Cell resistivity for charging(average)	R_c	1.1 Ωcm^2
Cell resistivity for discharging(average)	R_d	1 Ωcm^2
Container size	V_{con}	$4.66 \times 2.2 \times 2.42$ m^3
Inverter size (each one)	V_{inv}	$0.467 \times 0.61 \times 0.242$ m^3
Copper thermal conductivity (current collectors in stacks)	K_{co}	385 Wm^{-1}K^{-1}
Thickness of container walls	θ_{con}	0.005
Thickness of insulation materials	θ_{ins}	0.01 m

Table 2. Technical information of the FAP-450.

Parameter	Symbol	Value
Diffusion coefficient of V_{2+}	k_2	4.31×10^{-10} dm^2s^{-1}
Diffusion coefficient of V_{3+}	k_3	1.92×10^{-10} dm^2s^{-1}
Diffusion coefficient of V_{4+}	k_4	6.53×10^{-10} dm^2s^{-1}
Diffusion coefficient of V_{5+}	k_5	3.78×10^{-10} dm^2s^{-1}

3.2. Parameters of Heat Generation of Pumps and Inverters

In the simulations, six SMA inverters were utilised with an assumed efficiency of 95.8%. It was also assumed that the total output power of the 30 kW system was evenly distributed among the six inverters, and that the power losses of the inverters were all converted to heat. According to equations for heat generation calculation [6], the total amount of heat generated by the inverters can be determined, as shown below:

$$Q_{inverter} = 1315.24\,W \tag{11}$$

The MD-100R is typically selected for the purpose of electrolyte transfer, and the average flow rate is utilised in the calculation of heat. Details regarding heat generation for each pump are presented below:

$$Q_{pump}(each) = 80\,W \tag{12}$$

3.3. Active Cooling Power Consumption

For active cooling equipment operation, power consumption can be calculated using the heat removal rate ($Q_{active-cooling}$ in kW) and energy efficiency ratio (EER) in cooling. This is attributed to the fact that the EER represents the proportion of generated cooling energy to the consumed electrical energy under full load conditions [20]. Hence, to calculate the power consumption, the following equations can be used.

$$Power\ consumption = Q_{active-cooling}/EER \tag{13}$$

3.4. Hybrid Cooling Control Logic

For simulations involving only passive cooling, the hysteresis control logic from [6] was adopted (Algorithm 1). In the case of simulations using hybrid cooling (Algorithm 2), building upon the hysteresis control logic, a specific ambient temperature was set as the threshold for activating the air conditioning system, allowing the cooling strategy to switch between passive and active cooling seamlessly. This control logic allowed for the utilisation of passive cooling during periods of lower ambient temperatures to increase cooling efficiency. Furthermore, the activation of the air conditioning system or the fan system required satisfying separate conditions: the cold air temperature from the air conditioning system must be lower than the internal environment temperature of the container, and the ambient temperature must be lower than the air temperature inside the container.

Algorithm 1. Passive cooling only control logic

```
if (T_tank > T_air + ΔT and T_air−temperature−inside−container > T_air)
    if (T_tank > T_1)
        fan=on
    end
    if (T_tank < T_2)
        fan=off
    end
else
```

```
9        fan=off
10   end
```

Algorithm 2. Hybrid cooling control logic

```
1    if (T_tank > T_air + ΔT and T_air−temperature−inside−container > T_air)
2        if (T_tank > T_1)
3            fan=on
4        end
5        if (T_tank < T_2)
6            fan=off
7        end
8    else
9        fan=off
10   end
11   if T_air ≥ T_setting−ambient and T_air_in ≥ T_cold−air
12       Active Cooling = on
13   else
14       Passive Cooling = on
15   end
```

Since the temperature of the tank was easy to measure, it was used as the criterion for enabling passive cooling. Additionally, to increase the efficiency of the fan system, ΔT was introduced. Furthermore, by setting the threshold for the active cooling strategy ($T_{setting-ambient}$), the operating time of the air conditioning system was essentially determined. In summary, the active cooling strategy was activated when the ambient temperature (T_{air}) was greater than the threshold of the active cooling strategy ($T_{setting-ambient}$), and the air temperature inside the container (T_{air_in}) was higher than the cold air temperature from the air conditioning system. If the above conditions could not be met, but the tank temperature was higher than the ambient temperature by ΔT, the air temperature inside the container ($T_{air-temperature-inside-container}$) was higher than the ambient temperature, and the tank temperature was greater than the threshold set for passive cooling enable (T_1), the fan system was turned on and the air conditioning system did not work. As the passive cooling strategy took effect, the tank temperature dropped to below the threshold (T_2), the fan system was turned off, and both cooling systems were not working at this time. For other situations where cooling strategies were not required, neither system worked. In addition, the cooling strategy did not need to consider the level of air temperature inside the container. This was because the purpose of the cooling strategy was to ensure that the battery system operated within a safe temperature range.

3.5. Ambient Temperature Profile

Different ambient temperature scenarios were proposed in the case studies and these can be approximately described by using sinewave, which is shown below:

$$T_{ambient-temperature} = -0.5(T_{max} - T_{min})\sin(\omega t + \phi) + 0.5(T_{max} + T_{min}) \quad (14)$$

where T_{max} is the highest temperature of the day, ϕ is the phase shift, ω is the angular frequency and T_{min} is the lowest temperature of the day.

3.6. Load Profile

To enhance the relevance of the charging and discharging patterns for residential applications, the load profiles for 30 kW–180 kWh and 30 kW–240 kWh containerised systems are displayed in Figures 1–6, with consideration of different daylight PV charging.

These load profiles were designed to closely simulate typical usage patterns in various climates and geographical locations.

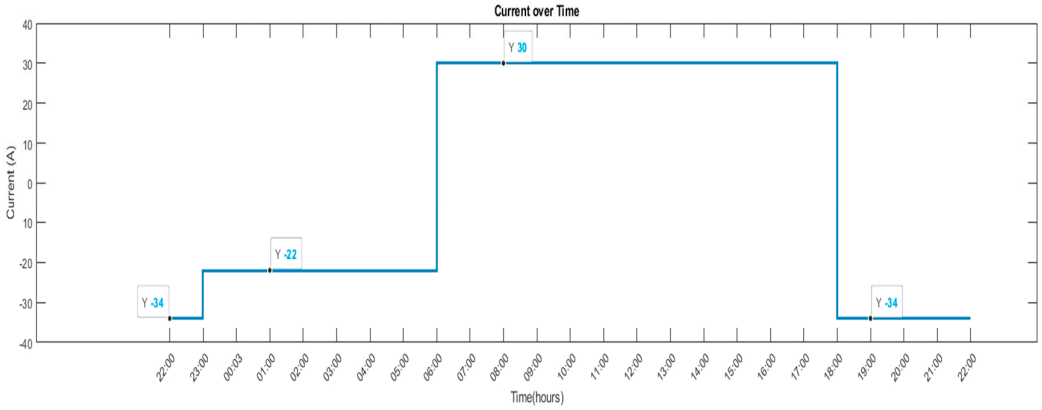

Figure 1. Current profile for the 6 h battery (temperate and hot climates−summer).

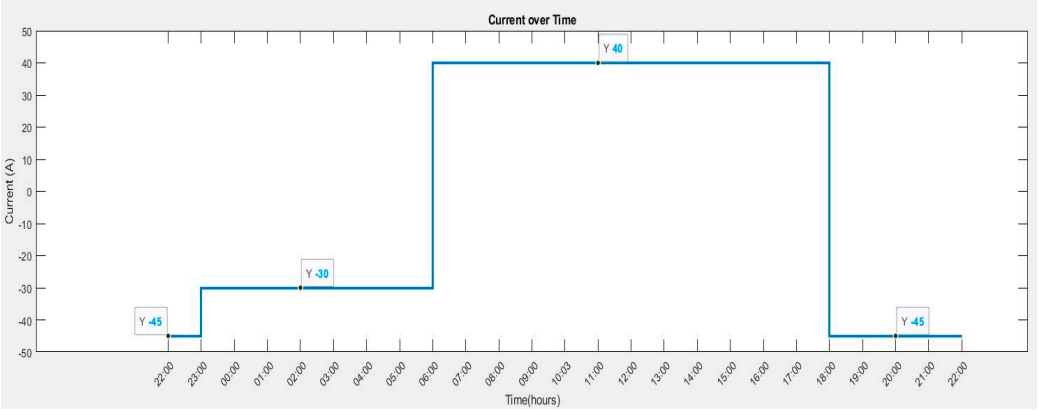

Figure 2. Current profile for the 8 h battery (temperate and hot climates−summer).

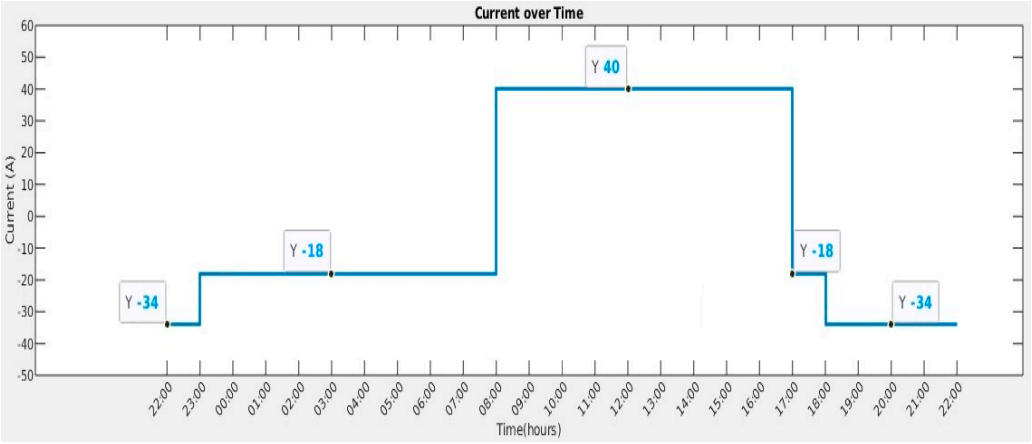

Figure 3. Current profile for the 6 h battery (temperate climate−winter).

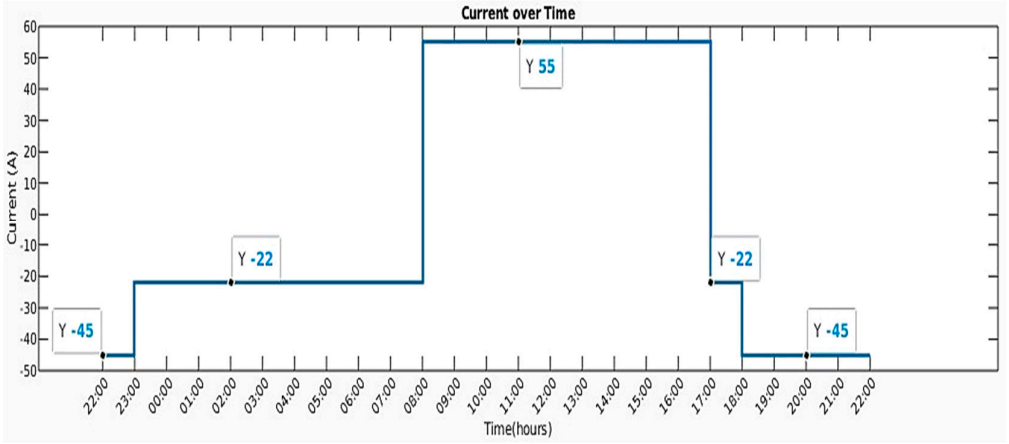

Figure 4. Current profile for the 8 h battery (temperate climate−winter).

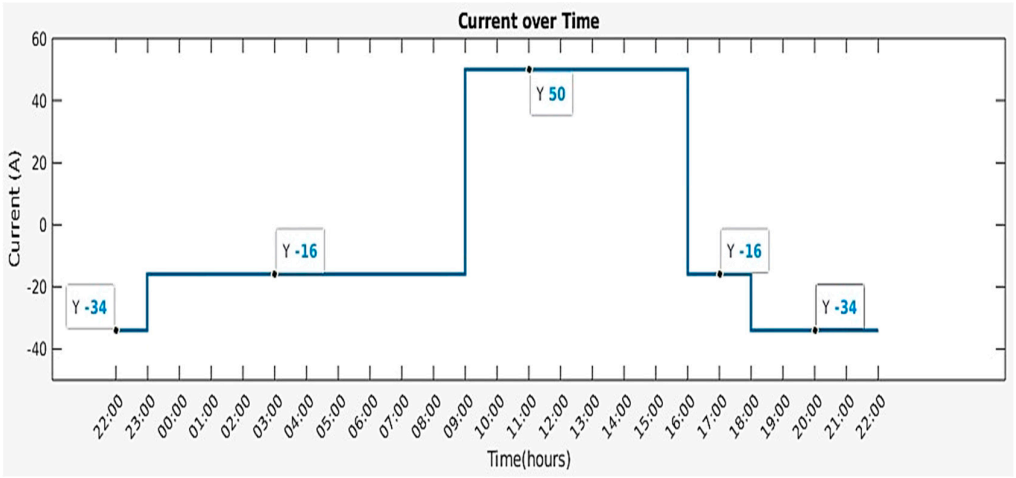

Figure 5. Current profile for the 6 h battery (high−latitude winter).

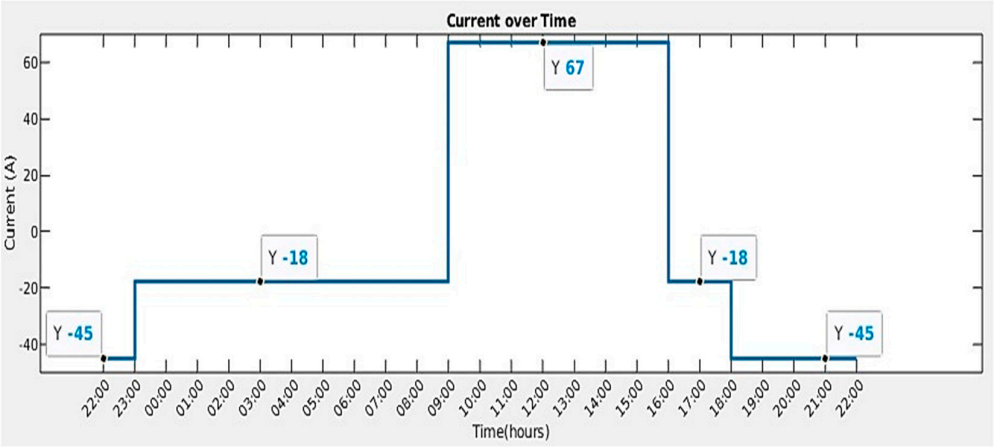

Figure 6. Current profile for the 8 h battery (high−latitude winter).

Because of variations in daytime duration across different regions and seasons, daytime plays a crucial role in determining the charging time for PV-related applications. This is because PV-related applications utilise solar energy to charge batteries. As a result, Figures 1–6 exhibit different charging times. Figures 1 and 2 illustrate the loading profiles of the 6 and 8 h systems in residential PV applications under a normal summer climate with

a 12 h daytime duration. Figures 3 and 4 show the loading profiles of the 6 and 8 h systems in residential PV applications in a typical winter climate with a 10 h daytime duration. Figures 5 and 6 depict the loading profiles of the 6 and 8 h systems in residential PV applications in high-latitude regions with only 7 h of daytime during winter.

3.7. Case Studies

Simulation results obtained from these case studies are presented here and discussed in detail. In addition, the effectiveness of hybrid cooling as a solution for managing temperature in these scenarios are also evaluated and applied when necessary. It was assumed that the lowest cold air temperature coming from the air conditioning system was typically 16 °C and the airflow rate remained constant while the active cooling system was operating. While the cooling control algorithm used in this study was by no means optimised, the results indicated the feasibility and ballpark energy consumption rates of the proposed hybrid cooling strategy.

3.7.1. Case 1: Normal Summer Climate

In this ambient temperature scenario, the main objective was to investigate the temperature response of the stacks and tanks when using containerised VFB systems in countries and regions where temperatures typically range from 15 °C to 35 °C during the summer. These countries and regions usually experience tropical, subtropical monsoon climates or Mediterranean climates. The load profiles in Figures 1 and 2 were used in this scenario.

Figure 7 illustrates that fan-based passive cooling was capable of adequately cooling the stacks and tanks in a 6 h containerised system. However, the presence of inverters led to excessive heat generation, resulting in further increases in the temperature of the stacks and tanks, ultimately reaching high levels. Therefore, it is highly recommended to isolate the inverters from the internal environment to prevent such temperature increases. Despite the fact that fan-based passive cooling was influenced by ambient temperatures, and that insulation materials limited heat dissipation, this cooling strategy remained effective when appropriate insulation materials were implemented.

For a 6 h containerised VFB system (30 kW–180 kWh):

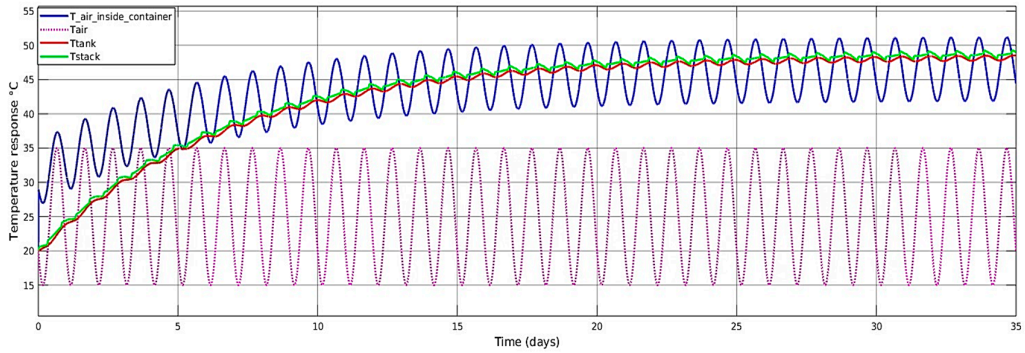

(**a**)

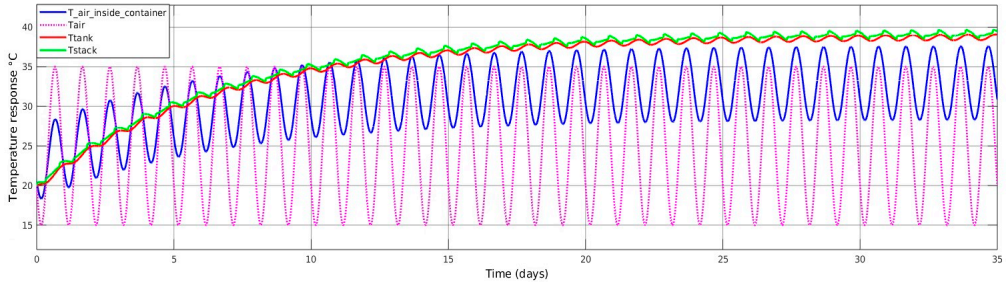

(**b**)

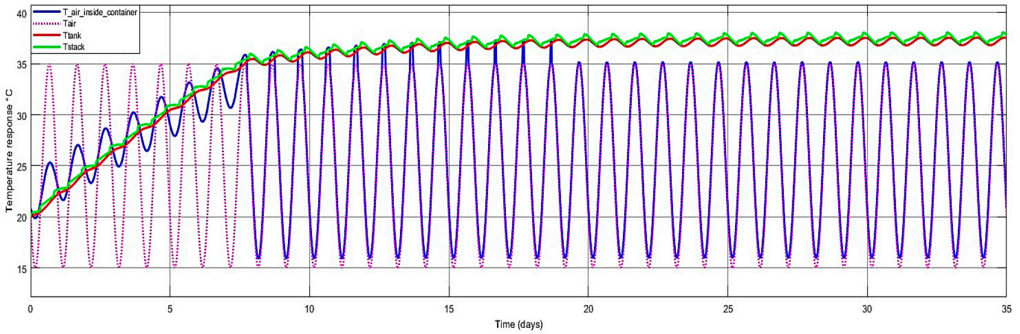

(**c**)

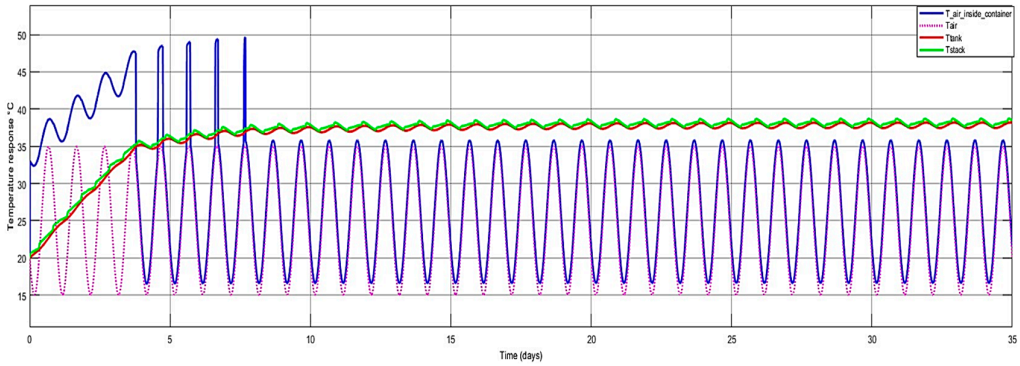

(**d**)

Figure 7. Temperature response for a 6 h containerised VFB using the FAP-450 membrane for ambient temperature between 15 °C and 35 °C: (**a**) without insulation and fans, inverters are not isolated ($Q_{inverter} = 1315.24\,W$); (**b**) without insulation and fans, inverters are isolated ($Q_{inverter} = 0\,W$); (**c**) with 0.02 m thick polyurethane insulation and passive cooling, inverters are isolated ($Q_{inverter} = 0\,W$); (**d**) with 0.02 m thick polyurethane insulation and passive cooling, inverters are not isolated ($Q_{inverter} = 1315.24\,W$).

As demonstrated in Figure 8, as the charging and discharging current increased, the issue of ohmic heating became increasingly prominent. This resulted in the final temperature of the stack and tank exceeding 40 °C. As illustrated in Figure 8b, even with the inverter being isolated and without self-discharge, the final temperatures of the stack and tank exceeded 40 °C, which posed a risk of V(V) precipitation in the positive electrolyte. Hence, the implementation of suitable hybrid cooling techniques was necessary to facilitate additional cooling of the stacks and tanks.

For an 8 h containerised VFB system:

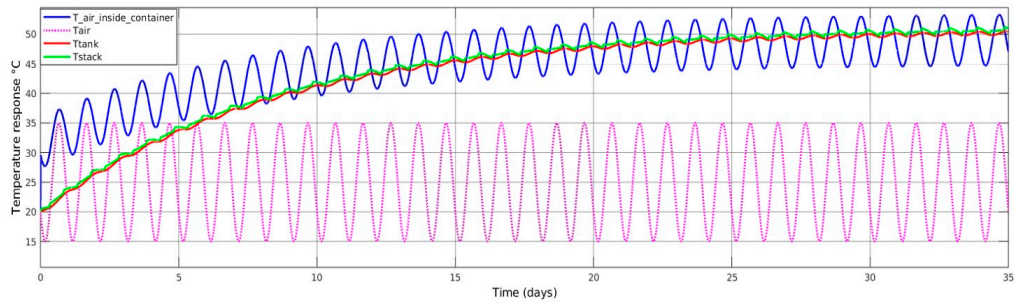

(**a**)

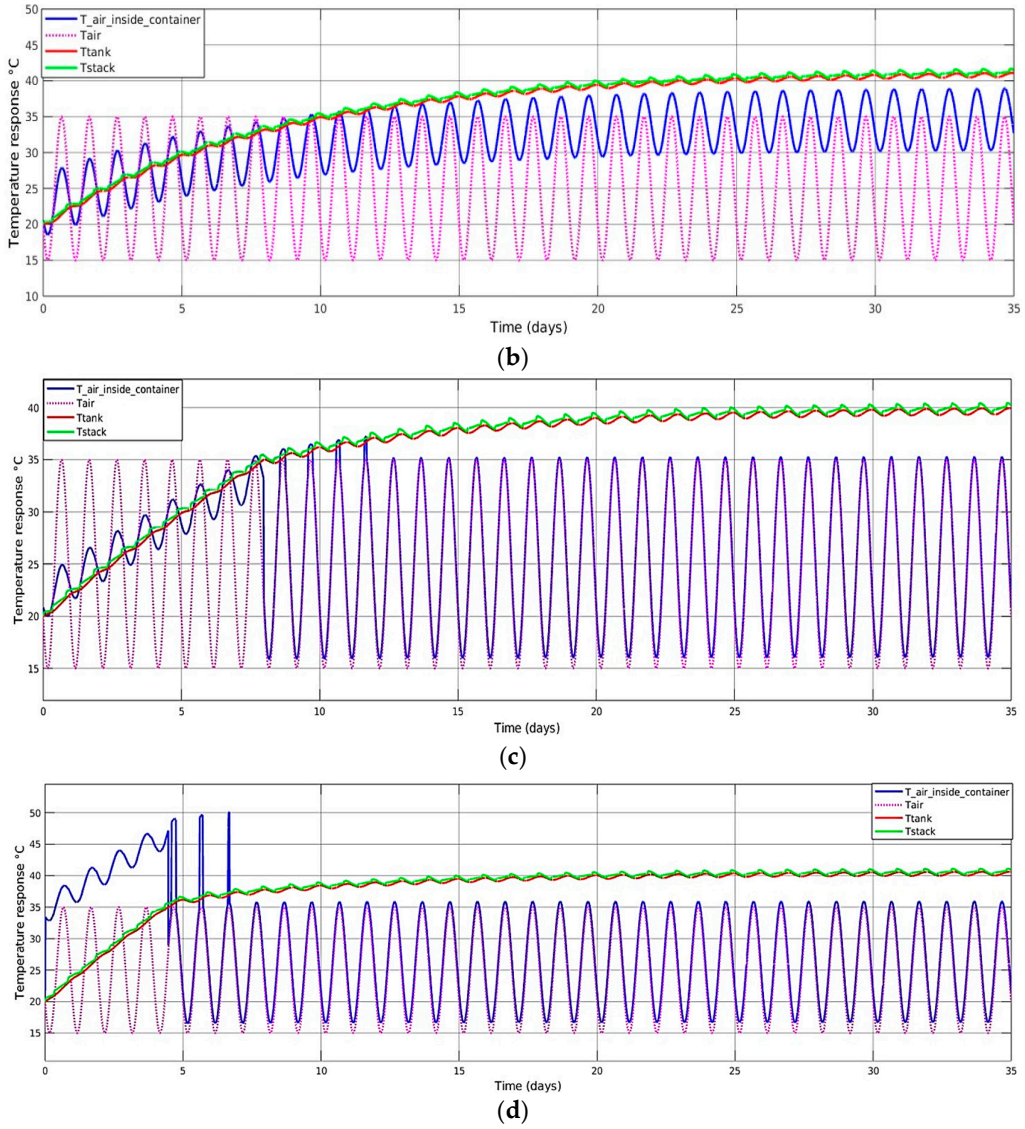

Figure 8. Temperature response for an 8 h containerised VFB using the FAP-450 membrane for ambient temperature between 15 °C and 35 °C: (**a**) without insulation and fans, inverters are not isolated ($Q_{inverter} = 1315.24\,W$); (**b**) without insulation and fans, inverters are isolated ($Q_{inverter} = 0W$); (**c**) with 0.02 m thick polyurethane insulation and passive cooling, inverters are isolated ($Q_{inverter} = 0W$); (**d**) with 0.02 m thick polyurethane insulation and passive cooling, inverters are not isolated ($Q_{inverter} = 1315.24W$).

For air conditioning systems, the cooling capacity provided by manufacturers was, in fact, the maximum possible heat removal rate. The power consumption based on this parameter also represented the maximum possible power consumption. This was not a suitable reference for a dynamic model. Additionally, the heat removal rate (kW) was influenced by the temperature difference between the air entering and leaving the air conditioning system. As this study adopted a mixed cooling mode, using the average value to evaluate the power consumption of the air conditioner during operation was more accurate.

Based on the results depicted in Figure 9, it was evident that an airflow rate of 1.0 m^3/s was insufficient to attain the desired air temperature of 25 °C inside the container. The final air temperature inside the container was approximately 26 °C. However, the internal temperature was not a matter of concern. The focus was solely on ensuring that the

temperature of the electrolyte in the stack and tank remained within the safe operation range.

Because of the set cold air temperature being 25 °C, which was much higher than the assumed minimum cold air temperature, and the operating duration being only 6 hours, the air conditioning system did not operate during the remaining 18 hours of each day. As shown in Figure 9c,d, the scenarios represented by Figure 9a,b had an average power consumption of less than 100 W over 30 days. Since the airflow rate in Figure 9b was lower, its average power consumption was approximately 68 W, as illustrated in Figure 9d. Additionally, from Figure 9c,d, it can be observed that the air conditioning systems with 1.0 m^3/s and 0.2 m^3/s airflow rates, when set to a cold air temperature of 25 °C for cooling this containerised VFB system, had maximum power consumptions of 973 and 4741 W, respectively. This was similar to the rated power consumption listed in the manufacturer's product information [21].

To achieve effective cooling and ensure the proper operation of the battery, a cooling strategy that combined the air conditioning system with a fan-based passive cooling strategy was applied, stabilising the final temperature of the stacks and tanks at approximately 37 °C with an airflow rate of 1.0 m^3/s (Figure 9a).

When the airflow rate was reduced to 0.2 m^3/s (Figure 9b), the maximum stack temperature reached about 38.9 °C. However, the cooling effect of the air conditioning system was noticeably worse compared to an airflow rate of 1.0 m^3/s, and the temperature was closer to the critical state. The air temperature inside the container when the air conditioner was turned on was approximately 28 °C. Therefore, it was worth considering increasing the airflow rate appropriately while also considering reducing the power consumption of the air conditioning system. A balance needed to be found between these two factors for this 8 h battery containerised system. The simulation results under two different airflow rates are given because the air conditioning system with an airflow rate between the two was easily found [21–23].

As the charging and discharging currents of the 8 h system were significantly higher than those of the 6 h system, the ohmic heating rates of the 8 h battery during charging and discharging processes were 266 and 537 W higher, respectively, compared to the 6 h system. Additionally, the increased electrolyte volume resulted in a larger thermal mass for the 8 h system. These factors collectively contributed to the distinct temperature responses observed between the 6 h and 8 h batteries.

For an 8 h containerised VFB system with feasible hybrid cooling:

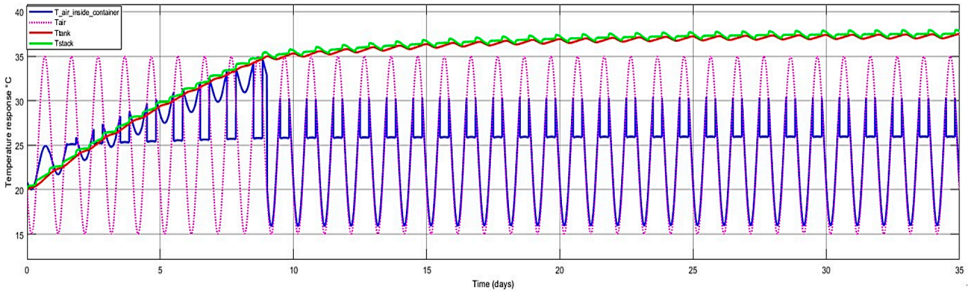

(**a**)

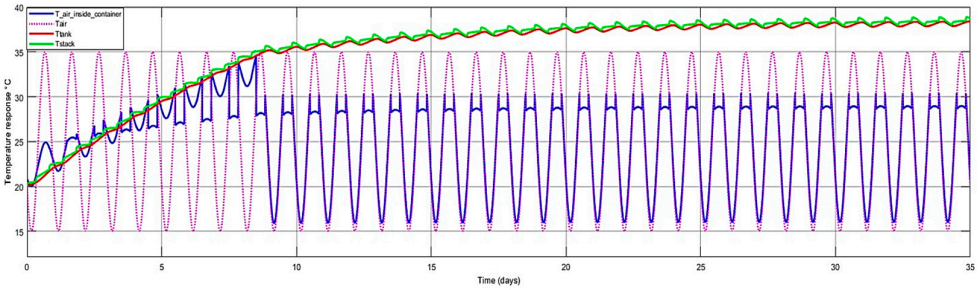

(**b**)

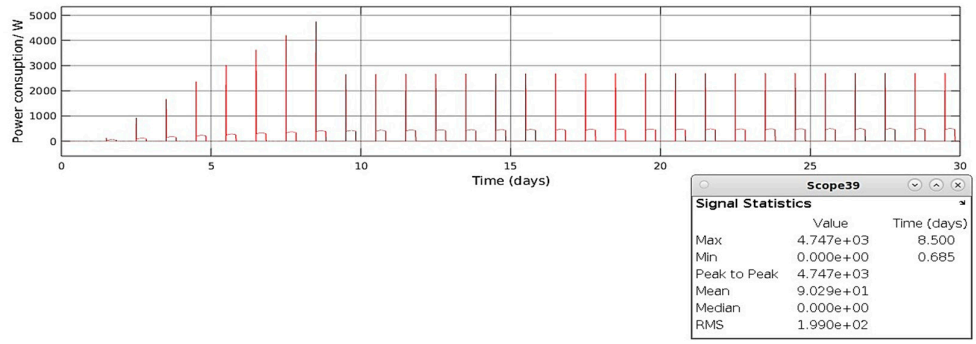

(**c**)

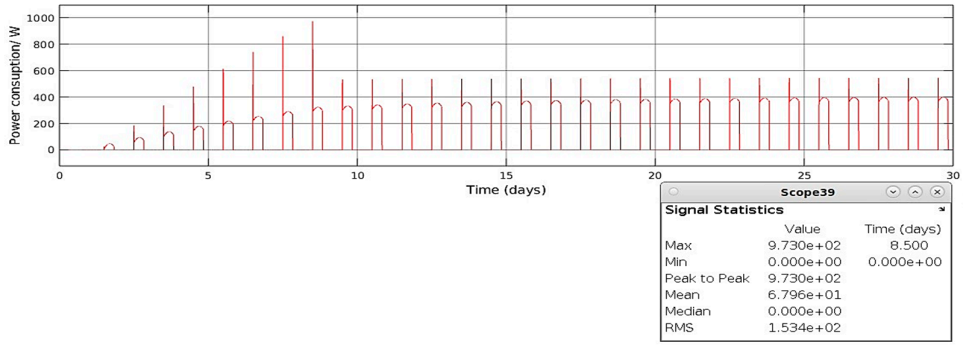

(**d**)

Figure 9. Temperature response for an 8 h containerised VFB using the FAP-450 membrane for ambient temperature between 15 °C and 35 °C with active cooling: (**a**) air conditioning system opens with an airflow rate of 1.0 m^3/s, $T_{ambient-temperature} \geq 30$ °C, and $T_{cold-air} = 25$ °C, passive cooling applied during the rest of the time every 24 h, with 0.02 m insulation; (**b**) air conditioning system opens with an airflow rate of 0.2 m^3/s(200 L/s), $T_{ambient-temperature} \geq 30$ °C and $T_{cold-air} = 25$ °C, passive cooling applied during the rest of the time every 24 h, with 0.02 m insulation; (**c**) power consumption under (**a**) condition; (**d**) power consumption under (**b**) condition.

3.7.2. Case 2: Temperate Climate—Normal Winter

In many temperate regions of the world, the temperature during winter is between 5 °C and 15 °C. These include tropical, subtropical monsoon climates or Mediterranean climates. In some high-latitude regions, this temperature range can also be observed during summers. Because of the reduced daylight hours in temperate regions during winter compared to temperate or hot summers, we could not apply the load profile from Figures 1 and 2 to this scenario. In addition, typical winter daylight hours in these regions typically fall between 8 am and 5 pm, so charging can only occur during these times. Consequently, for both 6 and 8 h batteries, their charging current will increase to accommodate the

shorter daylight duration. Furthermore, before the peak electricity demand arrives around 6 pm, most appliances in residential buildings are in standby mode. Therefore, during this time period, the batteries should operate in a low current discharge mode as reflected in the proposed load profile presented in Figures 3 and 4.

As shown in Figures 10 and 11, when the ambient temperature was between 5 °C and 15 °C and insulation was applied with a shorter daytime, the final temperature of the stack and tank in both the 6 h and 8 h systems could still be stabilised at no more than 35 °C using only passive cooling. Because of the shorter daytime, charging currents rose to 40 and 55 A for the 6 h and 8 h systems, respectively. It can also be seen from the figure that the temperature of the stack and tank in the 8 h system increased more quickly. Because of the higher efficiency of passive cooling at a lower ambient temperature and control logic threshold settings, the stack and tank temperature can be seen to switch between 25 °C and 35 °C in these two figures. Consequently, active cooling was deemed unnecessary for this scenario when operating the 6 h or 8 h containerised VFB system.

For a 6 h containerised VFB system (30 kW–180 kWh):

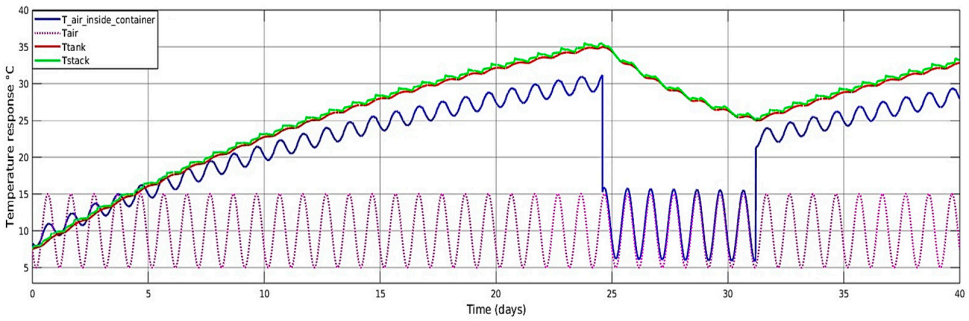

Figure 10. Temperature response of an 6 h system with only passive cooling, with 0.02 m thick polyurethane insulation material when the ambient temperature ranges from 5 °C to 15 °C, $Q_{inverter}$ = 0 W.

For an 8 h containerised VFB system (30 kW–240 kWh):

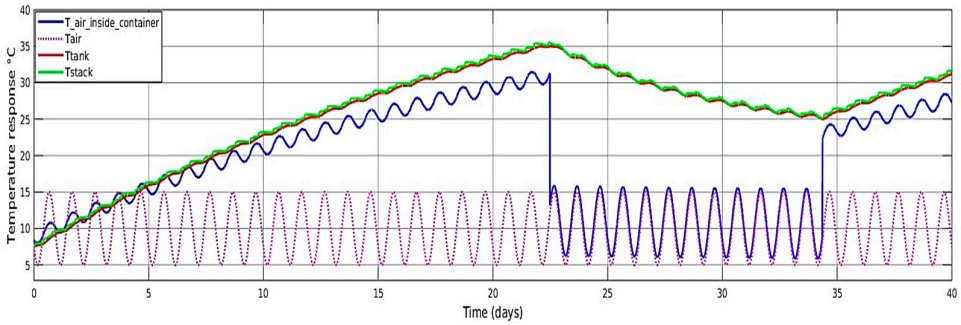

Figure 11. Temperature response of an 8 h system with only passive cooling, with 0.02 m thick polyurethane insulation material when the ambient temperature ranges from 5 °C to 15 °C, $Q_{inverter}$ = 0W.

3.7.3. Case 3: Extremely Cold Region Winter Climate

In high-latitude countries and regions, winter brings shorter daylight hours, and some may even experience polar nights. These areas typically exhibit sub-frigid coniferous forest climate, cold zone climate, or tundra climate, characterised by temperatures ranging below −10 °C. During the simulation, passive and active cooling were disabled, and initial temperature was set at 20 °C. Because of the shorter daylight hours in winter in high-latitude regions, the winter daylight duration is much shorter than the normal

winter scenario. The ambient temperature profile of the coldest day in Edmonton (Canada) [24] during December 2022 was chosen in the simulation, and daytime is typically between 9 am and 4 pm. This implied that batteries required a higher current in charging mode compared to the normal winter scenario. For the record, the temperature range was between −25 °C and −34 °C. From Figure 12 (top), when the inverters were isolated from the container, the 6 h system demonstrated a significant decrease in the stack and tank temperature, stabilising at below 0 °C. Consequently, in such a situation, the electrolyte is highly susceptible to freezing.

Figure 12 (bottom) illustrates that the stack and tank temperature for a 6 h containerised VFB system could be sustained at approximately 29.5 °C by incorporating inverters into the container. In this instance, the inverters also served as heaters to warm the interior environment of the container. As a result, the utilisation of inverters can reduce the requirement for active heating, resulting in energy cost savings for 6 h containerised VFB systems.

For a 6 h containerised VFB system(30 kW–180 kWh):

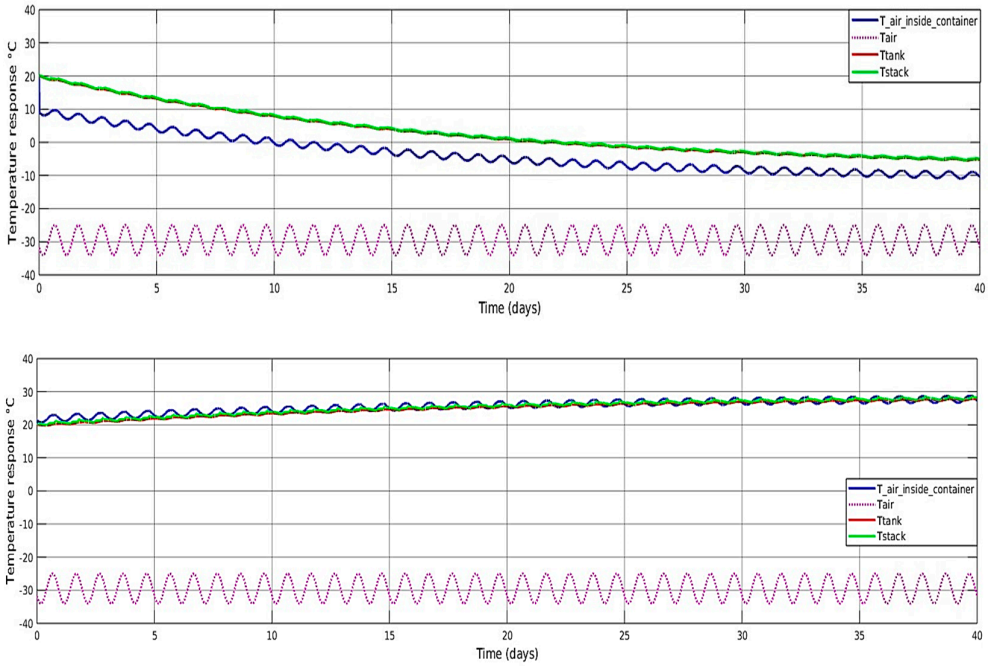

Figure 12. Temperature response of a 6 h system without any cooling, with 0.02 m thick polyurethane insulation material when the ambient temperature ranges from −34 °C to −25 °C, (**top**) $Q_{inverter} = 0\,W$, (**bottom**) $Q_{inverter} = 1315.24\,W$.

As seen in Figure 13a, by isolating inverters from the inner environment of the container, the stack and tank temperatures eventually stabilised at a value of 5 °C. This indicated that under this scenario, the vanadium electrolyte was at risk of reaching its freezing point.

Figure 13b illustrates the temperature response of the stack and tank when inverters were not isolated. In this scenario, the temperature of the stack and tank stabilised at around 38.5 °C at the end of the 40-day simulation, which was quite close to 40 °C, with a tendency to continue rising. Consequently, it is recommended that the inverter should be partially isolated from the inner environment of the container in such situations to maintain safe operation.

Figure 13c illustrates the temperature response of the stack and tank when half of the inverters were isolated, and the other half were not isolated. The stack and tank temperature eventually stabilised at around 20 °C. This suggested that for high-latitude regions,

it is still possible to maintain the crucial components within the container at a safe operating temperature without the use of cooling or heating equipment, simply by accommodating a portion of the inverters inside the container.

Compared to the temperature response of a 6 h battery under the same ambient temperature conditions, the 8 h battery exhibited this temperature response owing to the increase in the charging current, resulting in higher ohmic heating. In comparison to the 6 h battery, the ohmic heating of the 8 h battery was approximately 756 W greater during charging and about 392 W higher during discharging. Moreover, since the 8 h battery had a larger electrolyte volume, its thermal mass was also much greater compared to the 6 h battery. As a result, the stack and tank temperature of the 8 h battery displayed this particular trend.

For an 8 h containerised VFB system (30 kW–240 kWh):

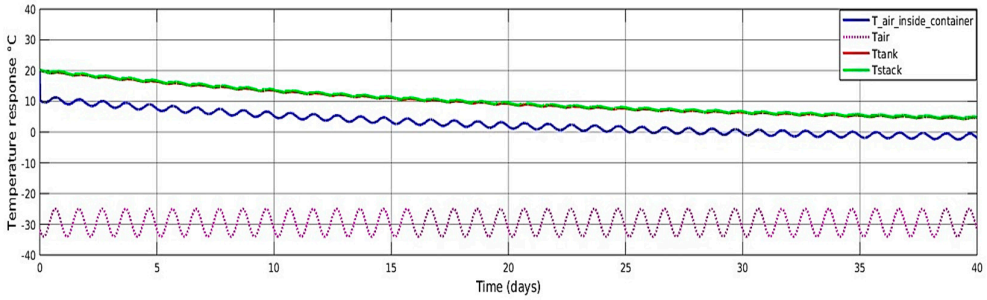

(**a**)

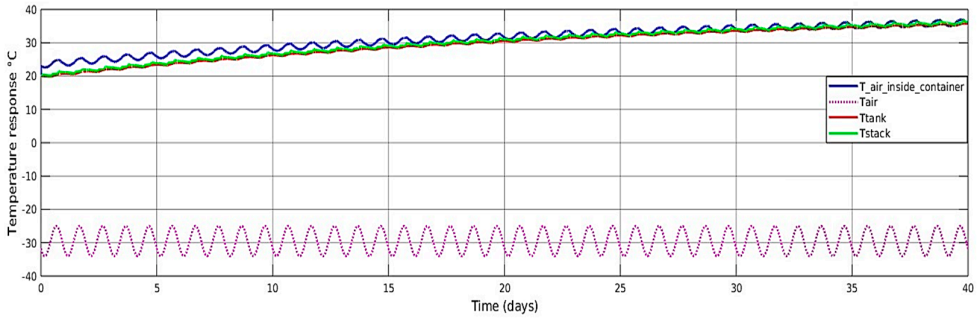

(**b**)

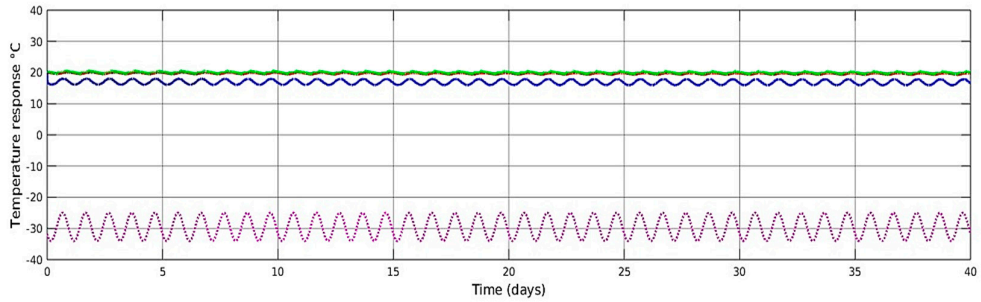

(**c**)

Figure 13. Temperature response of an 8 h system without any cooling, with 0.02 m thick polyurethane insulation material when the ambient temperature ranges from −34 °C to −25 °C: (**a**) $Q_{inverter}$ = 0 W; (**b**) $Q_{inverter}$ = 1315.24 W; (**c**) $Q_{inverter}$ = 657.62 W (half of the number of inverters are isolated).

3.7.4. Case 4: Hot Arid Climate

Under identical ambient temperature conditions and without insulation, the final temperature of the stacks and tanks proposed in [4] for a 30 kW–130 kWh system was observed to exceed 40 °C. As a result, to ensure the secure functioning of the containerised VFB system, introducing active cooling was imperative.

For a 4 h battery operating in an environment with temperatures between 25 °C and 45 °C, passive cooling was insufficient to maintain stack and tank temperatures below 40 °C. Therefore, for a 6 h containerised VFB system, active cooling must be used to further reduce the temperature of the stacks and tanks. As shown in Figure 14a, when an air conditioning system with a flow rate of 1.0 m^3/s was activated during the hottest 12 h of the day and passive cooling was used for the remaining 12 h, the stack and tank temperature levelled around 39.9 °C. Thus, there was still a risk of electrolyte precipitation.

Figure 14b depicts the simulation results when the air conditioning system operated for 16 h, while all other conditions remained unchanged. This implied that the air conditioning system would be active during the hottest 16 h of the day, and passive cooling would be employed for the remaining time. The results showed that the final temperature of the stacks and tanks was approximately 36.5 °C. This significantly ensured the safe operation of the battery system and maintained relatively low power consumption. This setting provided a certain temperature buffer to keep the battery functioning properly, even if extreme environmental temperatures occurred during certain periods.

For a 6 h containerised VFB system with feasible hybrid cooling:

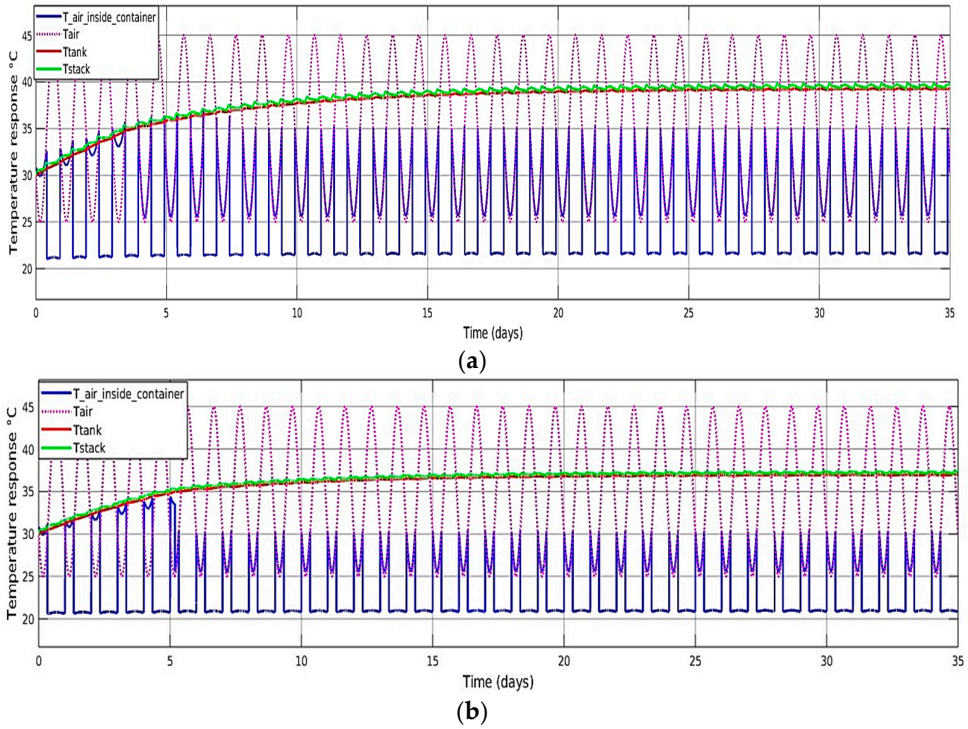

Figure 14. (**a**) Air conditioning system opens if necessary with an airflow rate of 1.0 m^3/s, $T_{ambient-temperature} \geq 35$ °C and $T_{cold-air} = 20$ °C, passive cooling applied during the rest of the time every 24 h, with 0.02 m insulation, $Q_{inverter} = 0$ W; (**b**) air conditioning system opens if necessary with an airflow rate of 1.0 m^3/s, $T_{ambient-temperature} \geq 30$ °C and $T_{cold-air} = 20$ °C, passive cooling applied during the rest of the time every 24 h, with 0.02 m insulation, $Q_{inverter} = 0$ W.

Figure 15a displays the simulation results for an 8 h battery with an air conditioning system active during the hottest 12 h of the day and passive cooling employed for the rest of the time, using a large airflow rate of 12.22 m^3/s. Unfortunately, even with such a high

airflow rate, the final temperature of the stacks and tanks reached 41.5 °C, which could not ensure the safe operation of the battery.

Figure 15b shows increasing the air conditioning system's operating time to 16 h while reducing the airflow rate to 1.6 m^3/s compared to Figure 15a. The final temperature of the stacks and tanks in Figure 15a,b was similar. Although the final temperature still exceeded 40 °C, the system's demand for the air conditioning airflow rate significantly decreased because of the increase in the air conditioning system operation time.

Figure 15c is based on the condition in Figure 15b but reduced the cold air temperature from the air conditioning system to 16 °C. The final temperature of the stacks and tanks was approximately 37.5 °C, significantly lower than before, which ensured the safe operation of the battery. Therefore, appropriately adjusting cold air temperature from the air conditioning system can effectively decrease the temperature of the stacks and tanks.

For an 8 h containerised VFB system with feasible hybrid cooling:

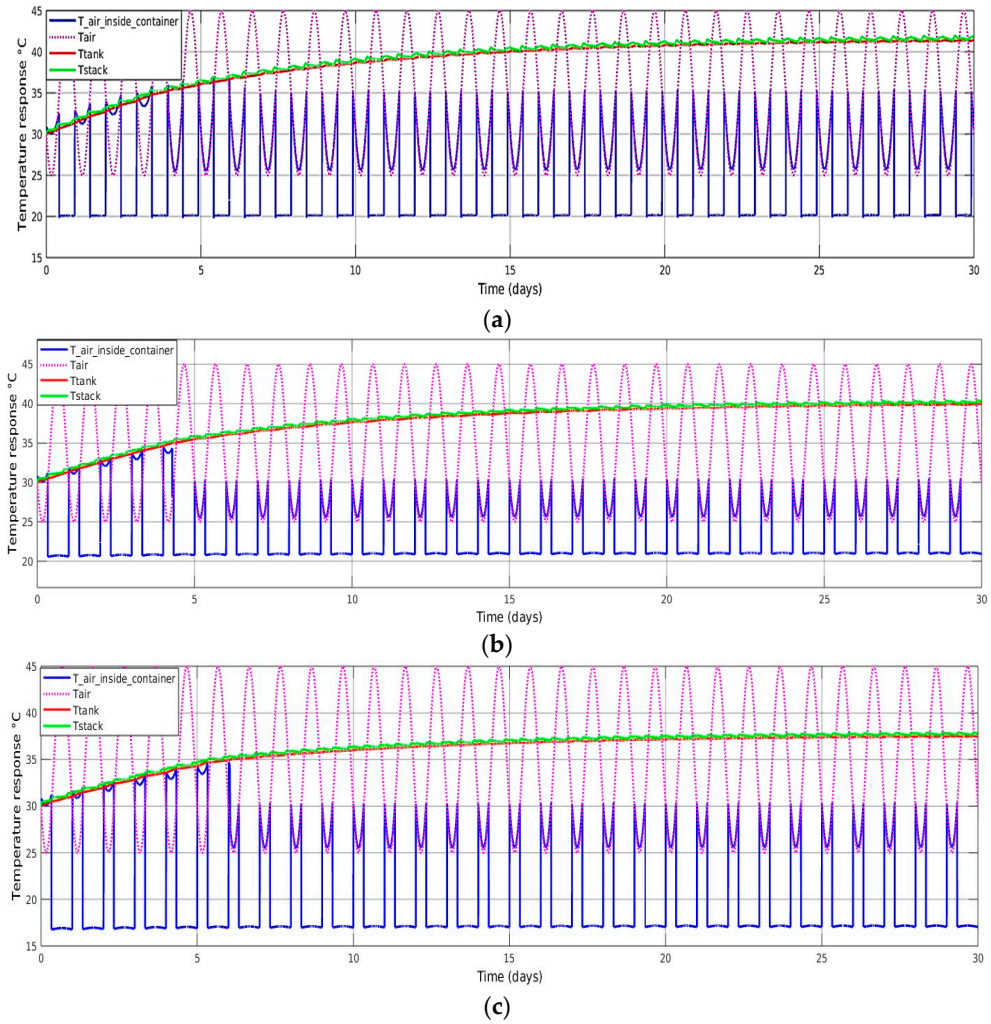

Figure 15. (**a**) Air conditioning system opens if necessary with an airflow rate of 12.22 m^3/s, $T_{ambient-temperature} > 35$ °C and $T_{cold-air} = 20$ °C, passive cooling applied during the rest of the time every 24 h, without insulation, $Q_{inverter} = 0$ W; (**b**) air conditioning system opens if necessary, with an airflow rate of 1.6 m^3/s, $T_{ambient-temperature} \geq 30$ °C and $T_{cold-air} = 20$ °C, passive cooling applied during the rest of the time every 24 h, with 0.02 m insulation, $Q_{inverter} = 0$ W; (**c**) air conditioning system opens if necessary with an airflow rate of 1.6 m^3/s, $T_{ambient-temperature} \geq 30$ °C and $T_{cold-air} = 16$ °C, passive cooling applied during the rest of the time every 24 h, with 0.02 m insulation, $Q_{inverter} = 0$ W.

Figure 16 displays the power consumption of the air conditioning system over a 30-day period. As the power consumption was not constant, the mean value was employed to better reflect the actual power consumption situation. Compared to Figure 16b, the results in Figure 16a suggested that it is not advisable to blindly pursue a higher air conditioning system airflow rate, as the high flow rate air conditioning system with a shorter operating time consumes more power. Since the simulation conditions for Figure 15b,c only differed in the temperature of the cold air supplied by the air conditioning system, and Figure 16 shows that the average power consumption for Figure 15c condition was higher, it can be reasonably inferred that if the cold air temperature in Figure 15a were set to 16 °C and the air conditioning system operating time further extended, the stack and tank temperatures could be reduced to below safe operation range, but the power consumption would further increase, thereby raising operational costs.

The conditions in Figure 15b,c utilised lower airflow rates, and by extending the air conditioning system's operating time, their cooling effects were superior to that shown in Figure 15a. Compared to Figure 15b, by decreasing the temperature of the cold air from the air conditioning system, the stack and tank temperature was maintained below 38 °C. However, this setting also increased the power consumption to some extent. Even with such a setting, the average power consumption was 458 W or 10.99 kWh energy consumption over a 24-h period, which was still a relatively small value for a 30 kW–240 kWh containerised VFB system. Additionally, the results from Figure 15a,b indicated that compared to pursuing a higher airflow rate, increasing the operating time of the air conditioning system proved to be more beneficial for the cooling effect.

Furthermore, although applying an airflow rate of 12.22 m^3/s resulted in a maximum power consumption of around 104 kW (Figure 16a), the average power consumption of this air conditioning system for a containerised 30 kW–240 kWh VFB system over 30 days was 563 W or 13.51 kWh energy consumption over a 24 h period. This implied that the electricity costs incurred from this condition were still relatively low.

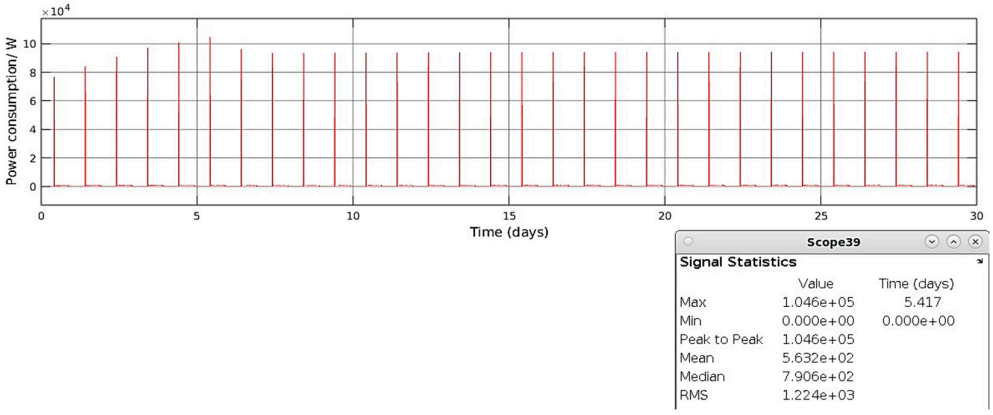

(**a**)

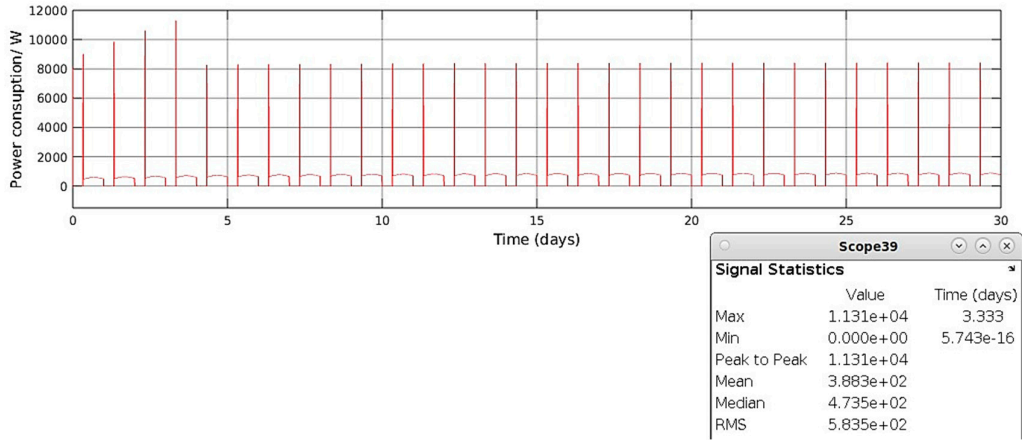

(**b**)

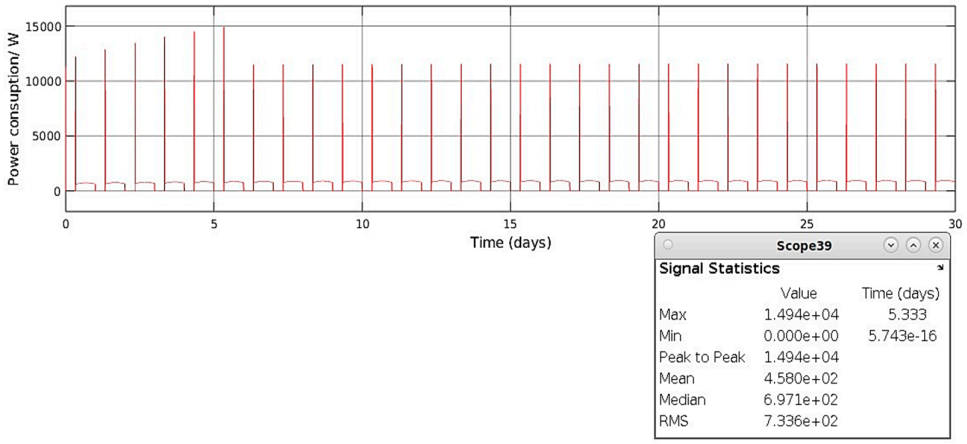

(**c**)

Figure 16. Average power consumption of the air conditioning system (**a**) under Figure 15a condition, (**b**) under Figure 15b condition, (**c**) under Figure 15c condition.

3.8. Discussion

The case study section investigated the temperature response of the important internal components of the 6 and 8 h batteries in various typical climates and provided active cooling solutions when passive cooling was insufficient to keep the stack and tank temperature below the safe operating temperature. At the same time, the power consumption of active cooling was analysed in detail. Additionally, different regions experience varying sunlight duration across different seasons. This study took this factor into account by adopting different load profiles in various scenarios, thereby more accurately reflecting real-world conditions. The average power consumption of air conditioning systems was used to evaluate the power consumption during long-term operation of air conditioning on batteries, allowing for a more accurate estimation of the energy consumption of the air conditioning system. This paper proposed a hybrid cooling strategy that ensures cooling effectiveness while keeping the operating cost of the containerised VFB system low, providing insights into the design of economically effective containerised vanadium flow battery thermal management systems, especially for countries and regions with extreme weather conditions. In addition, the loading profiles based on continuous charge and discharge discussed in this paper conformed to the characteristics of PV-connected residential applications and effectively eliminated the influence of self-discharge during standby periods on the stack and tank temperature inside the system.

4. Conclusions

The purpose of this work was to evaluate the thermal control requirements and the need for passive/active cooling of VFB systems for renewable applications (particularly with PV energy generation) under various climate conditions in different geographical locations, which are useful to battery designers and manufacturers. The simulation results indicated that active cooling is only necessary for the 6 h battery system when the ambient temperature exceeds 25 °C–45 °C or higher. For the 8 h system, active cooling is required when the ambient temperature is above 15 °C–35 °C. In extreme cold environments, the heat generated by inverters is necessary for the 6 h system to maintain the temperature of the stack and tank within safe operating ranges. Because of the specific load profile dictating that an 8 h system operating in high-latitude regions requires a charging current of 67 A, ohmic heating will be significant. Additionally, the thermal mass of the electrolyte is approximately 1.5 times larger compared to the 6 h system. As a result, the stack and tank temperature may exceed the safe operating range when inverters are not isolated. Therefore, it is recommended to isolate a portion of the inverters, maintaining the stack and tank temperature at around 20 °C. This approach provides more buffering capacity in the event of sudden temperature fluctuations. The primary differences in thermal behaviour between the 6 and 8 h systems under other conditions stem from the larger electrolyte volume in the 8 h system, resulting in a greater thermal mass, and the increased ohmic heating generated by the 8 h system owing to higher charging and discharging currents. These factors together contribute to the distinct thermal characteristics of the 8 h system compared to the 6 h system. By analysing different load profiles, it was also discovered that when using a containerised VFB system in winter, to ensure uninterrupted peak-time electricity consumption, users need to turn off more standby electrical appliances during off-peak periods. This allows the discharging current to be maintained at a lower level during off-peak times, thus ensuring adequate power availability during peak demand.

Moreover, merely increasing the airflow rate of the air conditioning system is not an economically efficient thermal management strategy, as the simulation results indicated that the power consumption of a high airflow rate system operating for less time was greater than that of a low airflow rate system operating for longer periods. Therefore, balancing the airflow rate with the air conditioning operating time and adjusting the cold air temperature can ensure that the stack and tank temperatures of the containerised VFB remain within safe working temperature ranges while reducing the power consumption of active cooling to a lower level.

Furthermore, the simulation results indicated that the system's average power consumption was not only affected by the airflow rate of the air conditioning system but also by the temperature difference between the air temperature inside the container and the cold air supplied by the air conditioning system, as well as the operating time of the air conditioning system. When an air conditioning system with a large airflow rate operates during a period where the temperature difference between the current temperature inside the container and the cold air supplied by the air conditioning system reaches its peak, the real-time power consumption of the air conditioning system will reach its maximum value. Additionally, based on the conversion of Dubai's residential electricity prices to Australian dollars (0.12 AUD/kWh), the electricity bill for the air conditioning system in the scenario shown in Figure 15c was approximately AUD 39.57 (329.75 kWh) per month.

Author Contributions: Conceptualization, B.S. and M.S.-K.; methodology, B.S.; software, B.S.; validation, B.S., M.S.-K., J.B. and K.M.; formal analysis, B.S., M.S.-K., J.B., and K.M.; investigation, B.S., M.S.-K., J.B. and K.M.; resources, B.S.; data curation, B.S.; writing—original draft preparation, B.S.; writing—review and editing, B.S., M.S.-K., J.B. and K.M.; visualization, B.S.; supervision, M.S.-K., J.B., and K.M.; project administration, J.B.; funding acquisition, J.B. All authors have read and agreed to the published version of the manuscript.

Funding: This project was partially funded by the Australian Research Council Research Hub for Integrated Energy Storage Solutions IH180100020.

Data Availability Statement: Data is unavailable due to privacy or ethical restrictions.

Conflicts of Interest: The authors declare no conflict of interest.

References

1. Sun, C.; Negro, E.; Vezzú, K.; Pagot, G.; Cavinato, G.; Nale, A.; Bang, Y.H.; Di Noto, V. Hybrid inorganic-organic proton-conducting membranes based on speek doped with wo3 nanoparticles for application in vanadium redox flow batteries. *Electrochim. Acta* **2019**, *309*, 311–325.
2. Tang, A.; Ting, S.; Bao, J.; Skyllas-Kazacos, M. Thermal modelling and simulation of the all-vanadium redox flow battery. *J. Power Sources* **2012**, *203*, 165–176.
3. Tang, A.; Bao, J.; Skyllas-Kazacos, M. Thermal modelling of battery configuration and self-discharge reactions in vanadium redox flow battery. *J. Power Sources* **2012**, *216*, 489–501.
4. Yan, Y.; Li, Y.; Skyllas-Kazacos, M.; Bao, J. Modelling and simulation of thermal behaviour of vanadium redox flow battery. *J. Power Sources* **2016**, *322*, 116–128.
5. Trovo, A.; Saccardo, A.; Giomo, M.; Guarnieri, M. Thermal modeling of industrial-scale vanadium redox flow batteries in high-current operations. *J. Power Sources* **2019**, *424*, 204–214.
6. Shu, B.; Weber, L.S.; Skyllas-Kazacos, M.; Bao, J.; Meng, K. Thermal modelling and simulation studies of containerised vanadium flow battery systems. *Batteries* **2023**, *9*, 196.
7. Trovo, A.; Guarnieri, M. Standby thermal management system for a kw-class vanadium redox flow battery. *Energy Convers. Manag.* **2020**, *226*, 113510.
8. Wei, Z.; Zhao, J.; Xiong, B. Dynamic electro-thermal modeling of all-vanadium redox flow battery with forced cooling strategies. *Appl. Energy* **2014**, *135*, 1–10.
9. Bhattacharjee, A.; Saha, H. Development of an efficient thermal management system for vanadium redox flow battery under different charge-discharge conditions. *Appl. Energy* **2018**, *230*, 1182–1192.
10. Rahman, F.; Skyllas-Kazacos, M. Vanadium redox battery: Positive half-cell electrolyte studies. *J. Power Sources* **2009**, *189*, 1212–1219.
11. Mohamed, M.; Leung, P.; Sulaiman, M. Performance characterization of a vanadium redox flow battery at different operating parameters under a standardized test-bed system. *Appl. Energy* **2015**, *137*, 402–412.
12. Zhang, C.; Zhao, T.; Xu, Q.; An, L.; Zhao, G. Effects of operating temperature on the performance of vanadium redox flow batteries. *Appl. Energy* **2015**, *155*, 349–353.
13. Skyllas-Kazacos, M.; Kazacos, M. State of charge monitoring methods for vanadium redox flow battery control. *J. Power Sources* **2011**, *196*, 8822–8827.
14. Prifti, H.; Parasuraman, A.; Winardi, S.; Lim, T.M.; Skyllas-Kazacos, M. Membranes for redox flow battery applications. *Membranes* **2012**, *2*, 275–306.
15. Carvalho, W.M., Jr.; Cassayre, L.; Quaranta, D.; Chauvet, F.; El-Hage, R.; Tzedakis, T.; Biscans, B. Stability of highly supersaturated vanadium electrolyte solution and characterization of precipitated phases for vanadium redox flow battery. *J. Energy Chem.* **2021**, *61*, 436–445.
16. Manufacturer, Fap-450. Available online: https://www.fuelcellstore.com/fumasep-fap (accessed on 10 February 2023).
17. Maghsoudy, S.; Rahimi, M.; Dehkordi, A.M. Investigation on various types of ion-exchange membranes in vanadium redox flow batteries: Experiment and modeling. *J. Energy Storage* **2022**, *54*, 105347.
18. Cho, H.; Krieg, H.M.; Kerres, J.A. Performances of anion-exchange blend membranes on vanadium redox flow batteries. *Membranes* **2019**, *9*, 31.
19. Li, Y.; Sun, L.; Cao, L.; Bao, J.; Skyllas-Kazacos, M. Dynamic model based membrane permeability estimation for online soc imbalances monitoring of vanadium redox flow batteries. *J. Energy Storage* **2021**, *39*, 102688.
20. Cengel, Y. *Thermodynamics: An Engineering Approach, McGraw-Hill Series in Mechanical Engineering*; McGraw-Hill Education: New York, NY, USA, 2014.
21. Manufacturer, Daikin Air Conditioning System. Available online: https://www.daikin.com.au/ (accessed on 15 March 2023).
22. Manufacturer, Hitachi Air Conditioning System. Available online: https://www.hitachiaircon.com/au (accessed on 20 March 2023).
23. Manufacturer, Mitsubishi Air Conditioning System. Available online: https://mhiaa.com.au/ (accessed on 22 March 2023).
24. Manufacturer, Weather Data. Available online: https://www.visualcrossing.com/weather/weather-data-services (accessed on 24 March 2023).